Low-loss sharp bends in polymer waveguides enabled by the introduction of a thin metal layer

Mustafa Akin Sefunc,[1,2,*] Markus Pollnau,[1] and Sonia M. García-Blanco[1,2]

[1]*Integrated Optical MicroSystems Group, MESA + Institute for Nanotechnology, University of Twente, P.O. Box 217, 7500 AE Enschede, The Netherlands*

[2]*Optical Sciences Group, MESA + Institute for Nanotechnology, University of Twente P.O. Box 217, 7500 AE Enschede, The Netherlands*

[*]*m.a.sefunc@utwente.nl*

Abstract: Embodying a thin metallic layer underneath the core of a sharply bent polymer waveguide is shown in this work to considerably reduce the total losses of both the quasi-transverse-electric and quasi-transverse-magnetic modes. The computational results show a total loss as low as ~0.02 dB/90° for the quasi-transverse-electric mode for radii between 6 and 13 μm at the wavelength of 1.55 μm, which corresponds to a 10-fold improvement over the purely dielectric counterpart. The radii range exhibiting such low total loss can be tuned by properly selecting the parameters of the structure. For the quasi-transverse-magnetic mode, the metal layer reduces the total losses modestly for radii ranging from 3 to 10 μm. Simulation results for different structural parameters are presented.

OCIS codes: (130.0130) Integrated optics; (130.2790) Guided waves; (160.3900) Metals; (240.6680) Surface plasmons; (250.5403) Plasmonics; (130.5460) Polymer waveguides.

References and links

1. L. Eldada and L. W. Shacklette, "Advances in polymer integrated optics," IEEE J. Sel. Top. Quantum Electron. **6**, 54–68 (2000).
2. H. Ma, A. K. Y. Jen, and L. R. Dalton, "Polymer-based optical waveguides: materials, processing and devices," Adv. Mater. **14**(19), 1339–1365 (2002).
3. B. Yang, L. Yang, R. Hu, Z. Sheng, D. Dai, Q. Liu, and S. He, "Fabrication and characterization of small optical ridge waveguides based on SU-8 polymer," J. Lightwave Technol. **27**(18), 4091–4096 (2009).
4. L. Jin, J. Wang, X. Fu, B. Yang, Y. Shi, and D. Dai, "High-Q microring resonators with 2 × 2 angled multimode interference couplers," IEEE Photon. Technol. Lett. **25**(6), 612–614 (2013).
5. Y. Shi, C. Zhang, H. Zhang, J. H. Bechtel, L. R. Dalton, B. H. Robinson, and W. H. Steier, "Low (sub-1-Volt) halfwave voltage polymeric electro-optic modulators achieved by controlling chromophore shape," Science **288**(5463), 119–122 (2000).
6. Y. Yang, M. B. J. Diemeer, C. Grivas, G. Sengo, A. Driessen, and M. Pollnau, "Steady-state lasing in a solid polymer," Laser Phys. Lett. **7**(9), 650–656 (2010).
7. X. Gong, M. Tong, Y. Xia, W. Cai, J. S. Moon, Y. Cao, G. Yu, C. L. Shieh, B. Nilsson, and A. J. Heeger, "High-detectivity polymer photodetectors with spectral response from 300 nm to 1450 nm," Science **325**(5948), 1665–1667 (2009).
8. Q. Xu, D. Fattal, and R. G. Beausoleil, "Silicon microring resonators with 1.5-μm radius," Opt. Express **16**, 4310–4315 (2008).
9. Y. Deki, T. Hatanaka, M. Takahashi, T. Takeuchi, S. Watanabe, S. Takaesu, T. Miyazaki, M. Horie, and H. Yamazaki, "Wide-wavelength tunable lasers with 100 GHz FSR ring resonators," Electron. Lett. **43**(4), 225–226 (2007).
10. S. I. Bozhevolnyi, V. S. Volkov, E. Devaux, J. Y. Laluet, and T. W. Ebbesen, "Channel plasmon subwavelength waveguide components including interferometers and ring resonators," Nature **440**(7083), 508–511 (2006).
11. T. Holmgaard and S. I. Bozhevolnyi, "Theoretical analysis of dielectric-loaded surface plasmon-polariton waveguides," Phys. Rev. B **75**(24), 245405 (2007).
12. T. Holmgaard, Z. Chen, S. I. Bozhevolnyi, L. Markey, and A. Dereux, "Dielectric-loaded plasmonic waveguide-ring resonators," Opt. Express **17**(4), 2968–2975 (2009).
13. T. Holmgaard, J. Gosciniak, and S. I. Bozhevolnyi, "Long-range dielectric-loaded surface plasmon-polariton waveguides," Opt. Express **18**(22), 23009–23015 (2010).
14. M. Z. Alam, J. Meier, J. S. Aitchison, and M. Mojahedi, "Super mode propagation in low index medium," in Conference on Lasers and Electro-Optics/Quantum Electronics and Laser Science Conference and Photonic Applications Systems Technologies, OSA Technical Digest Series (CD) (Optical Society of America, 2007), paper JThD112.

#198328 - $15.00 USD Received 26 Sep 2013; revised 15 Nov 2013; accepted 17 Nov 2013; published 25 Nov 2013

15. M. Z. Alam, J. Meier, J. S. Aitchison, and M. Mojahedi, "Propagation characteristics of hybrid modes supported by metal-low-high index waveguides and bends," Opt. Express **18**(12), 12971–12979 (2010).
16. R. F. Oulton, V. J. Sorger, D. A. Genov, D. F. P. Pile, and X. Zhang, "A hybrid plasmonic waveguide for subwavelength confinement and long-range propagation," Nat. Photonics **2**(8), 496–500 (2008).
17. D. J. Dikken, M. Spasenović, E. Verhagen, D. van Oosten, and L. K. Kuipers, "Characterization of bending losses for curved plasmonic nanowire waveguides," Opt. Express **18**(15), 16112–16119 (2010).
18. W. Wang, Q. Yang, F. Fan, H. Xu, and Z. L. Wang, "Light propagation in curved silver nanowire plasmonic waveguides," Nano Lett. **11**(4), 1603–1608 (2011).
19. A. V. Krasavin and A. V. Zayats, "Guiding light at the nanoscale: numerical optimization of ultrasubwavelength metallic wire plasmonic waveguides," Opt. Lett. **36**(16), 3127–3129 (2011).
20. D. F. P. Pile and D. K. Gramotnev, "Plasmonic subwavelength waveguides: next to zero losses at sharp bends," Opt. Lett. **30**(10), 1186–1188 (2005).
21. C. Yang, E. J. Teo, T. Goh, S. L. Teo, J. H. Teng, and A. A. Bettiol, "Metal-assisted photonic mode for ultrasmall bending with long propagation length at visible wavelengths," Opt. Express **20**(21), 23898–23905 (2012).
22. V. Krasavin and A. V. Zayats, "Three-dimensional numerical modeling of photonic integration with dielectric-loaded SPP waveguides," Phys. Rev. B **78**(4), 045425 (2008).
23. T. Holmgaard, Z. Chen, S. I. Bozhevolnyi, L. Markey, A. Dereux, A. V. Krasavin, and A. V. Zayats, "Bend- and splitting loss of dielectric-loaded surface plasmon-polariton waveguides," Opt. Express **16**(18), 13585–13592 (2008).
24. M. W. Kim and P. C. Ku, "Lasing in a metal-clad microring resonator," Appl. Phys. Lett. **98**(13), 131107 (2011).
25. H. S. Chu, Y. Akimov, P. Bai, and E. P. Li, "Submicrometer radius and highly confined plasmonic ring resonator filters based on hybrid metal-oxide-semiconductor waveguide," Opt. Lett. **37**(21), 4564–4566 (2012).
26. C. Horvath, D. Bachman, M. Wu, D. Perron, and V. Van, "Polymer hybrid plasmonic waveguide and microring resonators," IEEE Photon. Technol. Lett. **23**(17), 1267–1269 (2011).
27. D. Dai, Y. Shi, S. He, L. Wosinski, and L. Thylen, "Silicon hybrid plasmonic submicron-donut resonator with pure dielectric access waveguides," Opt. Express **19**(24), 23671–23682 (2011).
28. K. Y. Lee, N. LaBianca, S. A. Rishton, S. Zolgharnain, J. D. Gelorme, J. Shaw, and T. H.-P. Chang, "Micromachining applications of a high resolution ultrathick photoresist," J. Vac. Sci. Technol. B **13**(6), 3012–3016 (1995).
29. X. B. Phoeni, V., Enschede, The Netherlands (*www.phoenixbv.com*).
30. S. M. García-Blanco, M. Pollnau, and S. I. Bozhevolnyi, "Loss compensation in long-range dielectric-loaded surface plasmon-polariton waveguides," Opt. Express **19**(25), 25298–25311 (2011).
31. K. R. Hiremath, M. Hammer, R. Stoffer, L. Prkna, and J. Čtyroký, "Analytic approach to dielectric optical bent slab waveguides," Opt. Quantum Electron. **37**(1-3), 37–61 (2005).
32. E. D. Palik, *Handbook of Optical Constants of Solids* (Academic Press, 1985).

1. Introduction

Integrated optical devices in polymeric materials have been the subject of a great deal of research over the past couple of decades [1–4]. Advantages of polymer waveguides include low cost as well as flexibility and ease of fabrication. Polymer materials span a wide range of refractive index values and exhibit a large transparency window, which makes them compatible with many photonic technologies for a large range of applications. Furthermore, different active dopants can be added to the polymeric material to fabricate devices with electro-optical [5], optical gain [6], or detection [7] capabilities.

One of the main drawbacks of polymeric waveguides is the large radius of curvature, typically a few tens of micrometers [3, 4], required for low-loss propagation. This is due to the low refractive index contrast between core and cladding typically obtained in polymer waveguide structures. Smaller radii of curvature are highly desirable in integrated photonics as they permit decreasing device footprint. In devices such as ring resonators, a small radius not only decreases dimensions but can also potentially reduce power consumption in active devices, while providing a large free spectral range (FSR). The latter is an important parameter in the design of filters and modulators for WDM systems [8] as well as tunable lasers with a wide wavelength range and stable laser operation [9] in which a single resonance peak within the material gain bandwidth prevents mode hopping while permitting smooth wavelength tuning.

Plasmonic waveguides have been proposed as good candidates for very-high-scale integration of photonic devices thanks to their capability to achieve very tight light confinement, which permits increasing device density, while benefiting from the large bandwidth of photonic devices [10]. A trade-off between confinement and propagation losses, however, has until now limited the application of this type of waveguides in real-life devices.

#198328 - $15.00 USD Received 26 Sep 2013; revised 15 Nov 2013; accepted 17 Nov 2013; published 25 Nov 2013

In an attempt to decrease propagation losses while maintaining sub-wavelength confinement, different waveguide structures have been proposed such as dielectric-loaded surface plasmon waveguides [11, 12], long-range dielectric-loaded surface plasmon waveguides [13] and hybrid plasmonic waveguides [14–16]. The high electromagnetic field confinement in plasmonic structures permits the realization of bends with radii of only a few micrometers. Bends in channel grooved plasmonic waveguides [10], metallic nanowire waveguides [17–19], metal-dielectric-metal plasmonic waveguides [20], dielectric-loaded surface plasmon waveguides [11, 12, 21–23], metal-clad waveguides [24] and hybrid dielectric-loaded surface plasmon waveguides [25, 26] have been investigated with radii of a few micrometers. However, the reported total losses per 90 degree bend are still too high for practical applications. The limiting factor is typically the high propagation loss of the plasmonic waveguide structures. Krasavin *et al.* [19] proposed the use of optical gain to compensate bend losses, thereby increasing the transmission through the bend to more than 95% (~0.2 dB of signal loss) in dielectric-loaded surface plasmon waveguides. Dai *et al.* [27] proposed a silicon hybrid plasmonic waveguide design capable of very sharp bends with low losses per 90 degree bend. Total losses close to ~0.04 dB/90° were calculated for a bend radius of 1.2 μm for the transverse-magnetic (TM) fundamental mode.

In this work, the introduction of a thin metallic layer underneath the core of a polymer waveguide is shown to reduce the calculated total losses (dB/90°) of sharp bends with respect to the total losses of the equivalent dielectric structure (i.e., without the metallic layer) for a large range of bend radii. The loss reduction is especially significant for the quasi-transverse-electric (TE) mode, for which the metallic configuration exhibits lower total losses for radii below 35 μm. For the quasi-TE mode, losses as low as ~0.02 dB/90° have been calculated for a wide range of radii that can be tuned by properly selecting the parameters of the structure. Such decrease in total loss represents one order of magnitude reduction with respect to the total losses of the pure dielectric structure for the same radii range. In the case of the quasi-TM mode, the total losses of the metallic structure are smaller than those of the dielectric structure for radii ranging from 3 to 10 μm. Introduction of the thin metallic layer in the proposed structure reduces the optimum radius of curvature of polymer waveguides from tens of micrometers to less than 10 μm, thereby enabling the utilization of polymer waveguides in highly integrated optical circuits and in devices where very sharp bends are necessary, such as ring resonators with large FSR. In the following sections, a detailed study of the total losses of the proposed polymer dielectric-loaded hybrid metallic bent waveguides including the effect of different structural parameters and materials on the calculated total losses is presented.

2. Proposed structure

The schematic configurations of the waveguide geometries studied in this paper are shown in Fig. 1. The proposed structure corresponds to a dielectric-loaded hybrid plasmonic waveguide consisting of a polymer ridge separated from the metal underneath by a thin low refractive index dielectric layer. The material selected for the ridge is the negative tone epoxy resist SU-8 [28], although similar results apply to a wide range of architectures exhibiting low refractive index contrast between substrate and core. For high-index-contrast waveguide architectures introduction of the metal has a less beneficial effect on the propagation losses. The material of the thin buffer layer is SiO_2. Gold was selected for the metallic layer. The substrate consists of silicon with a sufficiently thick layer of thermal SiO_2. Figure 1(b) shows the cross-section of the entirely dielectric structure used as a benchmark. The dielectric-loaded hybrid plasmonic waveguide [Fig. 1(a)] will be referred to as “metallic” in the subsequent sections, whereas the dielectric polymer waveguide [Fig. 1(b)] will be called “non-metallic”. The effect of the thickness of the different layers, the dimensions of the ridge and the type of metal selected will be studied in the following sections. The corresponding optical properties of the different materials at the wavelength of interest (λ = 1.55 μm) as well as the ranges of parameters considered in this study are summarized in Table 1.

#198328 - $15.00 USD Received 26 Sep 2013; revised 15 Nov 2013; accepted 17 Nov 2013; published 25 Nov 2013

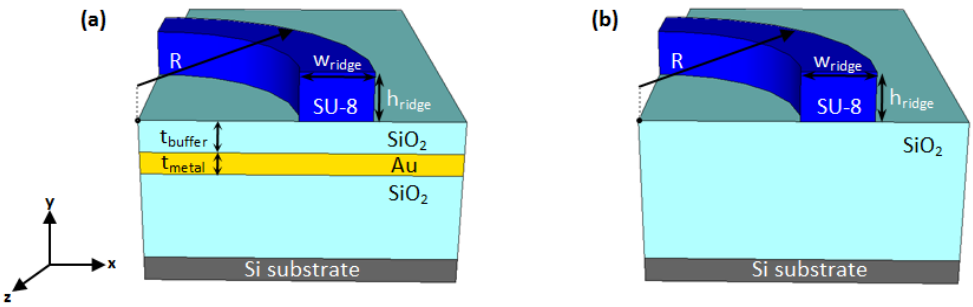

Fig. 1. (a) Dielectric-loaded hybrid plasmonic waveguide ("metallic" structure) and (b) dielectric reference structure ("non-metallic" structure). Typical parameters: $h_{ridge} = w_{ridge} = 2$ µm, $t_{buffer} = 100$ nm, $t_{metal} = 100$ nm. The silicon substrate was not taken into account in the simulations, as the thickness of the SiO_2 undercladding was considered sufficiently thick for the mode not to be influenced by the presence of the silicon substrate.

The distance between the center of curvature and the outer rim of the waveguide defines the bend radius, R, as depicted in Fig. 1. This definition of bend radius was chosen, because the outer rim is the important interface in very sharply bent waveguides, since the mode is pushed towards this boundary. Since disk resonators are devices which do not possess a waveguide width, defining the radius according to the outer interface will ensure compatibility of all the results.

Table 1. Refractive indices and thicknesses of the materials employed (λ = 1.55 µm).

	Material	Refractive index	Thickness (µm)
Undercladding	SiO_2	1.444	NA
Metal	Au	0.55 + i11.5	0.025-0.2
Buffer	SiO_2	1.444	0-0.4
Ridge	SU-8	1.57 + i4.93e-6	2
Uppercladding	Air	1	NA

3. Modeling of bent waveguides

Two-dimensional finite-difference (FD) calculations with perfectly matched layer (PML) boundary conditions were carried out using the FieldDesigner module of PhoeniX B.V [29]. for bend mode analysis. The fields were calculated in a sufficiently large calculation window (10 µm by 10 µm). Extra mesh grids were utilized for the thin metal and buffer layers to mitigate numerical errors in the calculations. The mesh override was implemented by artificially dividing the metal and buffer layers into 25 and 65 layers, respectively [30]. Scripts were written to find the guided modes of the structure iteratively for decreasing values of the bend radius. The loop first calculates the guided modes of the structure for a large radius of curvature. After each iteration step, the calculated effective refractive index is stored and set as target effective refractive index for the next iteration step and the value of the radius is decreased by a certain step size. For small radii (R < 35 µm), the effective refractive index changes faster than for large radii. In the calculation script, the step size of the radius is decreased when the iteration loop reaches low R values (threshold of R = 35 µm) to ensure that the calculation algorithm can find the correct guided mode. The total bend loss in a 90 degree bend of radius R can then be calculated from the imaginary part of the effective refractive index of the mode as Total Loss (dB/90°) = $10 \log_{10}[\mathrm{Im}(n_{eff})k_0 R\pi]$, where n_{eff} is the complex effective refractive index of the mode of the bent waveguide, k_0 is the wavenumber in vacuum ($k_0 = 2\pi/\lambda$) and R is the bend radius. It is important to note that this equation is independent of the definition of the bend radius (i.e., being the distance to either the rib center or the outer rim) as long as related values for n_{eff} and R are applied [31]. The calculated total loss includes both the propagation loss due to scattering and absorption in the metal and SU-8 material and the radiation loss due to the waveguide curvature (i.e., bend losses). In previous reports [17], the contribution of the bend losses to the total loss was extracted by assuming

#198328 - $15.00 USD Received 26 Sep 2013; revised 15 Nov 2013; accepted 17 Nov 2013; published 25 Nov 2013

that the propagation losses in the bent waveguide are identical to the propagation losses of the straight waveguide. Such an assumption is not possible in the structures of this work, as the mode profile changes considerably due to the bending, shifting towards the outer rim of the waveguide ridge (Fig. 2). Therefore, the reported losses throughout this paper are the total losses.

4. Study of bend losses as a function of radius for different parameters of the structure

In this comparative study, several structural parameters are taken into account to gain insight into their influence on the total losses of the bend. Such parameters comprise the ridge width (w_{ridge}) and height (h_{ridge}), buffer layer thickness (t_{buffer}), metal layer thickness (t_{metal}), and type of metal. The ridge width and height are each set to 2 μm to ensure single-mode operation (i.e., only one quasi-TE and one quasi-TM mode are supported by the structure).

Figure 2 depicts the real part of the dominant *E*-field component for the quasi-TE and quasi-TM modes supported by the non-metallic [Figs. 2(a) and 2(b)] and metallic [Figs. 2(c) and 2(d)] waveguide structures. It can be seen that the guided mode binds to the outer (right-hand side) rim of the ridge, since the turning is in the direction of the negative *x*-axis. The radius of curvature used in Fig. 2 is 6 μm. In the non-metallic structure, the generated leaky waves can be clearly observed and are due to the sharp bending of the waveguide. As the radius of curvature is further decreased, leakage into the substrate increases with the consequent reduction in mode intensity. This behavior translates into an augmentation of the bend losses for decreased radii of curvature, as can be seen in Fig. 3 (blue circles).

Introduction of a thin metallic layer underneath the polymer ridge blocks the radiation modes and pushes the quasi-TE mode towards the ridge in the positive *y*-axis direction [Fig. 2(c)]. Figure 3(a) shows the total losses per 90 degree bend for the metallic quasi-TE mode in comparison with those of the quasi-TE mode of the non-metallic structure. For large radii of curvature, the total losses per 90 degree bend of the metallic structure rise linearly with increasing radius. In this radius range, the total losses are dominated by the propagation losses and thus, they augment as the length of the 90 degree waveguide segment increases. When the radius decreases below a critical radius, the total losses rise again, this time due to the radiative losses introduced by the bend. It can be clearly seen in Fig. 3(a) that the introduction of the thin metal layer shifts the critical radius to a much lower value (i.e., ~7 μm) than in the non-metallic waveguide. Below a radius of ~35 μm, the total losses per 90 degree bend of the metallic structure are smaller than the ones of the non-metallic structure. This is particularly interesting for radii between 6 and 13 μm, where losses as low as 0.02 dB/90° have been calculated [inset of Fig. 3(a)].

The thin metallic layer underneath the polymer ridge transforms the photonic quasi-TM mode of the non-metallic structure [Fig. 2(b)] into a hybrid plasmonic-photonic mode. Such a mode is strongly coupled to the metal, thereby reducing leakage to the substrate and, therefore, the bend losses for small radii of curvature [Fig. 2(d)]. However, since the metal is highly absorptive at the wavelength of interest, high propagation losses are expected. High propagation losses are dominant for increasing radii [Fig. 3(b)]. A shift of the critical radius, below which the bend losses become dominant, to a smaller value than in the non-metallic structure still occurs despite the large propagation losses. For a narrow range of bend radii from 3 μm to 10 μm, the metallic structure exhibits lower total losses compared to the non-metallic counterpart [inset of Fig. 3(b)].

It is important to mention that the reduction of total bend losses (dB/90 degree bend) by the introduction of thin metal layers is larger for low refractive index contrast waveguides, for which the positive influence of usage of thin metal layers, i.e., by preventing the leakage, is higher than the negative effect of increased absorption introduced by the metal. High index contrast waveguide architectures show better confinement and less leakage to the substrate. For such structures, a thin metal layer has a lesser effect on blocking the radiation modes and pushing the guided mode towards the ridge, while the absorption of light due to the presence of the metal becomes significant.

#198328 - $15.00 USD Received 26 Sep 2013; revised 15 Nov 2013; accepted 17 Nov 2013; published 25 Nov 2013

The transition loss between a non-metallic straight waveguide and a metallic bend section have been investigated for the proposed waveguide architectures. The optimum offset values which provide maximum coupling efficiency have been calculated. Transition losses and optimum offset values depend on the particular waveguide parameters, the radius of curvature as well as the polarization. Typical transition losses are in the range of 0.8 dB to 1.5 dB per straight to bend connection. The transition losses are in the range of 0.1 dB to 1.3 dB for a non-metallic straight to a non-metallic bend waveguide section. The approach considered in this paper can also be applied to ring resonators in which no straight to bend connection is required.

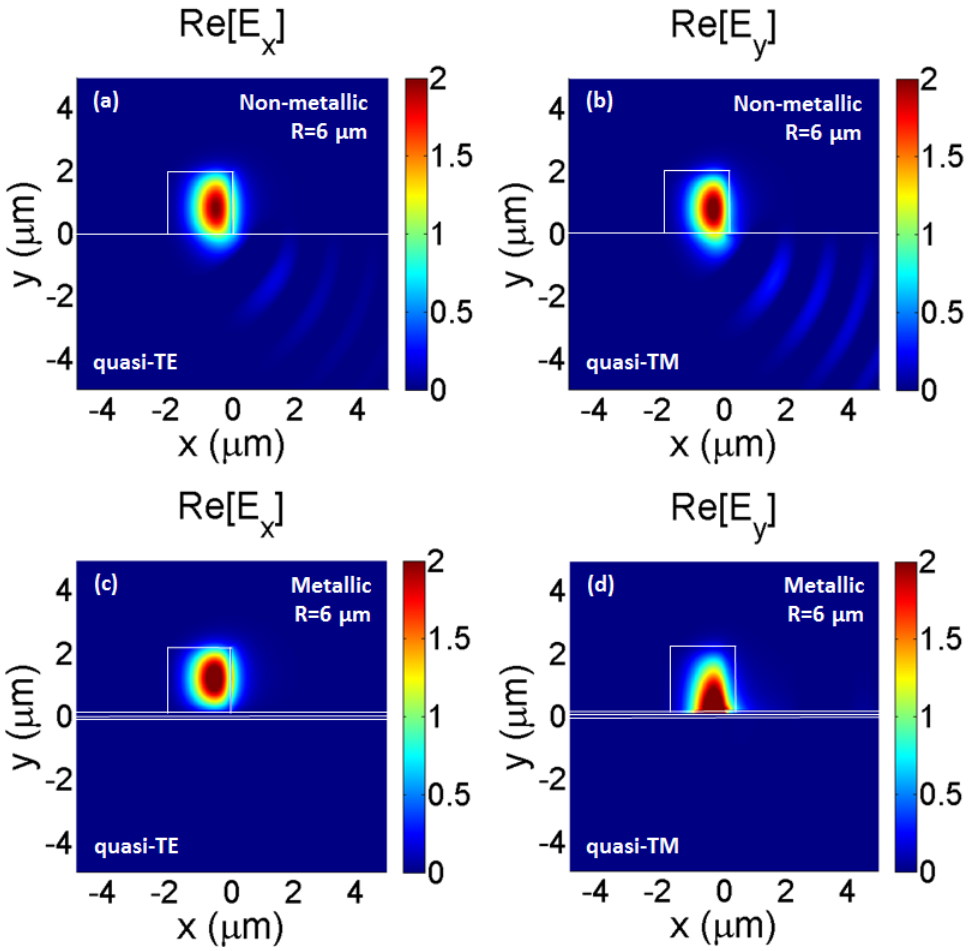

Fig. 2. Calculated 2-D mode profiles (showing the real part of the dominant electrical field component) at λ = 1.55 µm, R = 6 µm for the non-metallic structures (*top*) with the parameters of w_{ridge} = 2 µm, h_{ridge} = 2 µm for the (a) quasi-TE (Media 1) and (b) quasi-TM (Media 2) modes and for the metallic structures (*bottom*) with the parameters of w_{ridge} = 2 µm, h_{ridge} = 2 µm, t_{buffer} = 100 nm and t_{metal} = 100 nm for the (c) quasi-TE (Media 1) and (d) quasi-TM (Media 2) modes.

#198328 - $15.00 USD Received 26 Sep 2013; revised 15 Nov 2013; accepted 17 Nov 2013; published 25 Nov 2013

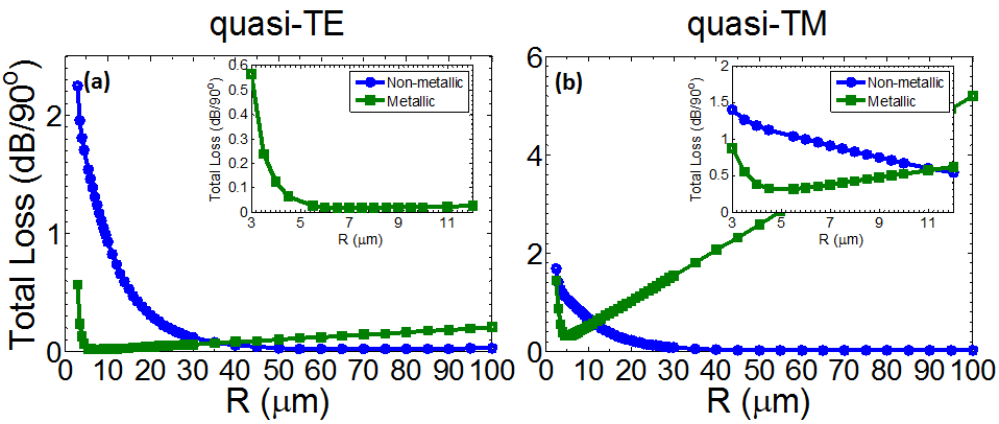

Fig. 3. Total loss (dB/90°) versus bend radius (R) for metallic and non-metallic structures for (a) quasi-TE and (b) quasi-TM modes with the parameters of w_{ridge} = 2 μm, h_{ridge} = 2 μm, t_{buffer} = 100 nm, and t_{metal} = 100 nm (only for metallic structure). The insets are a zoom of the corresponding loss plots in the region of interest.

4.1 Dependence of total losses on thickness of the buffer layer

The influence of the buffer layer thickness on the total losses has been investigated. The thickness of the buffer layer was varied between 0 nm and 400 nm. The losses per 90 degree bend for radii ranging from 2 μm to 30 μm were calculated for each value of buffer layer thickness. Results for the quasi-TE and quasi-TM modes are displayed in Fig. 4. As the thickness of the buffer layer augments, the critical radius for minimum losses per 90 degree bend shifts to larger radii. Increasing the buffer layer thickness has two consequences. For large bend radii, the losses per 90 degree go down as the thickness of the buffer layer augments. The field distribution is further away from the metal layer, therefore inducing less propagation losses for both quasi-TE and quasi-TM modes. For smaller radii (i.e., below the critical radius), as the buffer layer thickness increases, higher bend losses are obtained. Simultaneously, the critical radius shifts towards larger radii. In the case of the quasi-TE modes, this behavior can be explained as a reduction of the shield effect of the metal due to its larger distance from the mode [Fig. 5(c)]. For the quasi-TM modes, a thicker buffer layer enhances coupling of the bend mode to a surface plasmon mode supported by the layer structure outside the polymer ridge [Fig. 5(d)]. Figures 5(a) and 5(b) shows the mode profiles for quasi-TE and quasi-TM modes for a structure with no buffer layer.

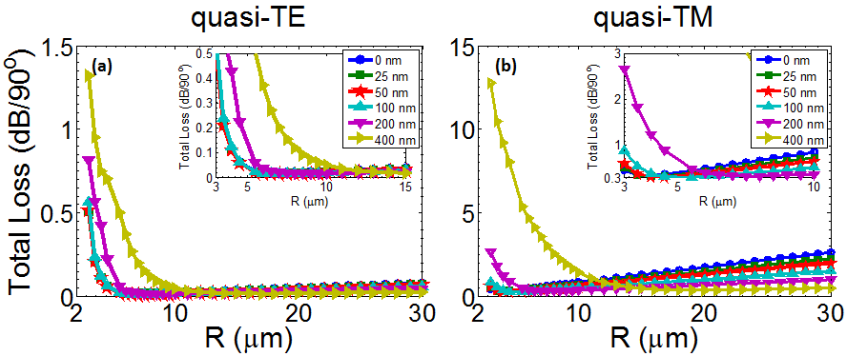

Fig. 4. Effect of the SiO_2 buffer thickness: Total losses (dB/90°) versus bend radius (R) for the metallic structure with the parameters of w_{ridge} = 2 μm, h_{ridge} = 2 μm, t_{metal} = 100 nm for different t_{buffer} parameter (t_{buffer} = 0 nm, 25 nm, 50 nm, 100 nm, 200 nm, and 400 nm) for (a) quasi-TE and (b) quasi-TM modes. The insets zoom in the regions of interest.

#198328 - $15.00 USD Received 26 Sep 2013; revised 15 Nov 2013; accepted 17 Nov 2013; published 25 Nov 2013

The thickness of the buffer layer is, therefore, a very important design parameter that permits shifting the range of radii where the lowest total losses occur. For example, no buffer layer would be preferred if the application requires the smallest radius possible. A thicker buffer layer would be preferred if low losses for slightly larger radii are desired. A 400 nm thick buffer layer enlarges the range of radii that exhibit total losses around ~0.02 dB/90° to between 13 and 25 μm for the parameters of the structure detailed in Fig. 4.

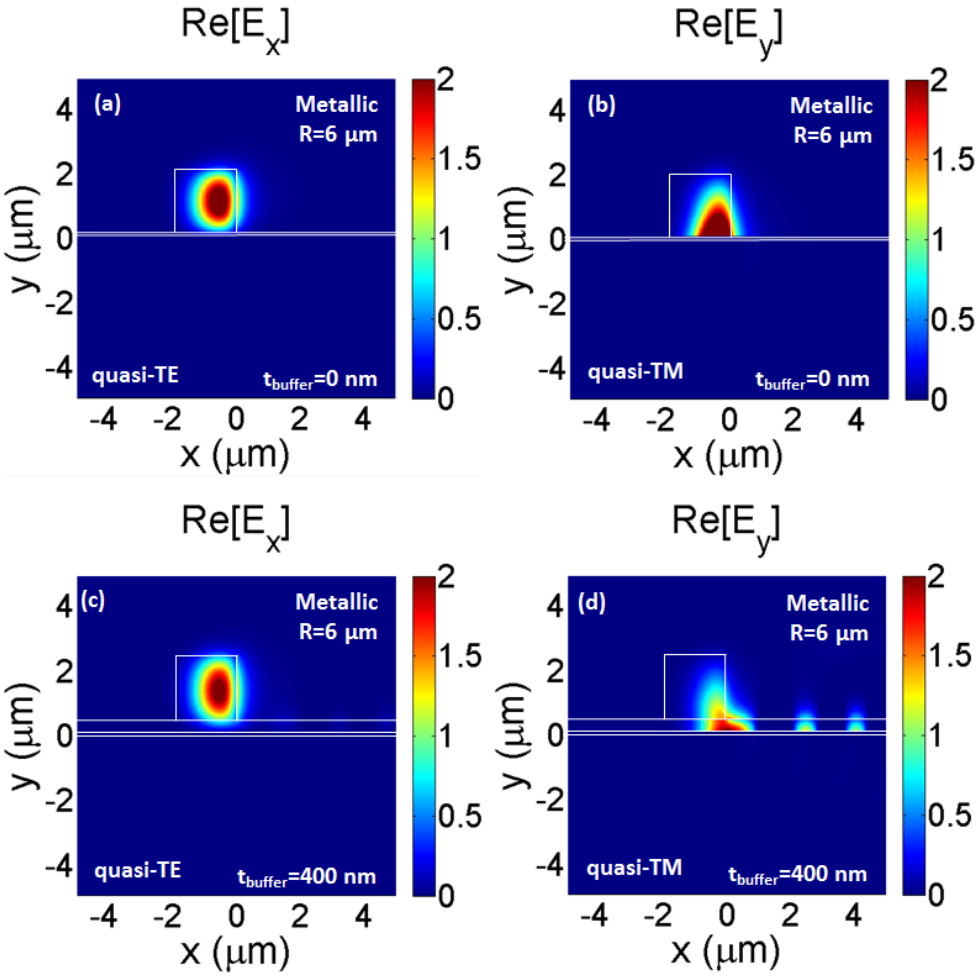

Fig. 5. Effect of the buffer layer thickness: Calculated 2-D mode profiles (shown as the real part of the dominant electrical field component) at λ = 1.55 μm, R = 6 μm for the metallic structure with the parameters of w_{ridge} = 2 μm, h_{ridge} = 2 μm, t_{metal} = 100 nm, t_{buffer} = 0 nm for the (a) quasi-TE (Media 3), (b) quasi-TM (Media 4) modes and in the case of t_{buffer} = 400 nm for (c) quasi-TE (Media 3) and (d) quasi-TM modes (Media 4).

4.2 Dependence of bend losses on metal layer thickness

The effect of the metal layer thickness was investigated. Figure 6 shows the total loss per 90 degree bend as a function of bend radius for both the quasi-TE [Fig. 6(a)] and the quasi-TM [Fig. 6(b)] modes. For the quasi-TE mode [Fig. 6(a)], provided the metal layer is sufficiently thick, it acts as a shield pushing the mode towards the ridge and preventing it from radiating to leaky waves in the substrate. This is the case for thicknesses above 50 nm. For thicknesses of the gold layer comparable to, or smaller than the penetration of the field in the metal layer,

#198328 - $15.00 USD Received 26 Sep 2013; revised 15 Nov 2013; accepted 17 Nov 2013; published 25 Nov 2013

coupling of the field to the substrate radiation modes can still occur, thereby increasing the contribution of the bend losses to the total loss per 90 degrees bend.

In the case of quasi-TM modes [Fig. 6(b)], as the metal thickness decreases, the mode binds more to the metal via excitation of surface plasmon modes on both surfaces of the metal layer. As a consequence, the propagation losses dramatically increase, as can be seen for gold layers thinner than 100 nm [Fig. 6(b)].

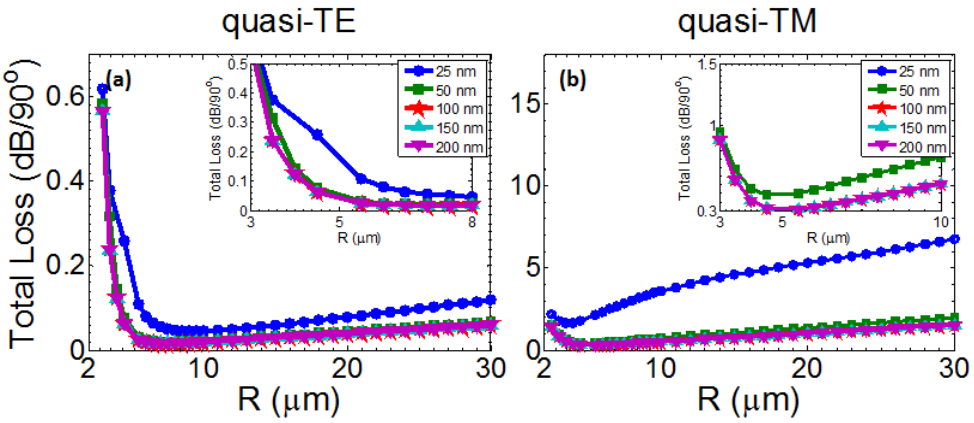

Fig. 6. Effect of metal thickness: Total loss (dB/90°) versus bend radius (R) for the metallic structure with the structural parameters of w_{ridge} = 2 μm, h_{ridge} = 2 μm, t_{buffer} = 100 nm for different t_{metal} (t_{metal} = 25 nm, 50 nm, 100 nm, 150 nm and 200 nm) for (a) quasi-TE and (b) quasi-TM modes. The insets are zoom of the corresponding loss plots.

4.3 Analysis of total loss dependence on metal type

According to the discussion in the previous sections, for the quasi-TE mode the metal layer acts like a shield that pushes the mode towards the ridge and prevents it from radiating into the substrate radiation modes. The shield effect is expected to become the more important, the more negative the real part of the metal dielectric permittivity is. Simultaneously, absorption in the metal increases with the imaginary part of the dielectric permittivity. Figure 7(a) shows the loss per 90 degree bend as a function of bend radius for four different metals (Al, Au, Ag, and Cu). The refractive indices and dielectric permittivity of these metals [32] at the wavelength of interest, λ = 1.55 μm, are shown in Table 2. For small radii the shield effect responsible for the reduction of losses per 90 degree bend is slightly larger for Al, followed by Au and Ag, the least performing metal being Cu. This is consistent with Al presenting the most negative real part of the dielectric permittivity and Cu the least negative one. For larger radii, Cu presents the highest propagation losses because the field is closer to the metal due to a less performing shield effect.

In the case of quasi-TM modes, the more negative the real part of the dielectric permittivity is, the lower are the propagation losses. This is in agreement with the results of the simulations, shown in Fig. 7(b).

Table 2. Refractive indices and dielectric permittivity of the metals employed in Fig. 7 (λ = 1.55 μm) [32].

Material	Refractive index	Dielectric permittivity
Al	1.44 + i*16	–253.93 + i*46.08
Au	0.55 + i*11.5	–131.95 + i*12.65
Ag	0.514 + i*10.8	–116.38 + i*11.10
Cu	0.606 + i*8.26	–67.86 + i*10.01

#198328 - $15.00 USD Received 26 Sep 2013; revised 15 Nov 2013; accepted 17 Nov 2013; published 25 Nov 2013

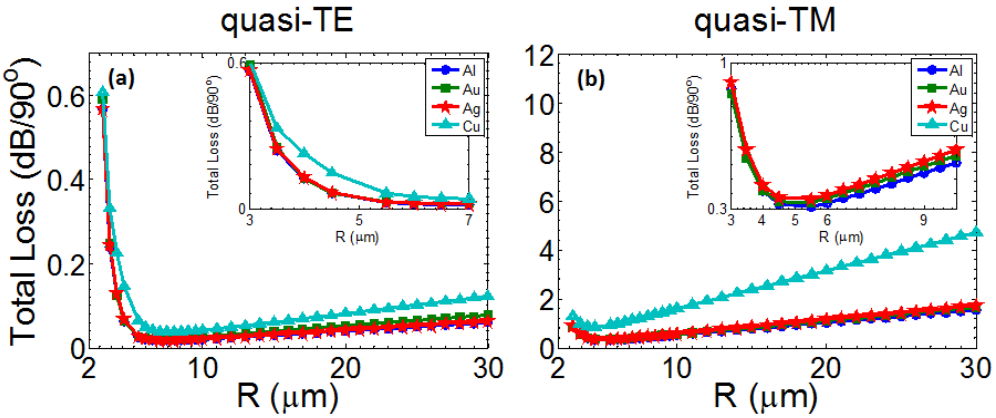

Fig. 7. Effect of metal type: Total loss (dB/90°) versus bend radius (R) for the metallic structure with the structural parameters of w_{ridge} = 2 μm, h_{ridge} = 2 μm, t_{metal} = 100 nm, t_{buffer} = 100 nm for different metals; Au, Ag, Al, Cu for (a) quasi-TE and (b) quasi-TM modes. The insets magnify the regions of small radii R.

5. Conclusions

In this work, we proposed and demonstrated numerically that introducing a thin metal layer underneath the core of a polymer waveguide permits the realization of sharp bends with calculated total losses (dB/90°) smaller than those of the equivalent dielectric waveguide without the metallic layer, both for quasi-TE and quasi-TM modes. The FD mode calculations indicate more than a 10-fold reduction of the bend losses with respect to the entirely dielectric structure for radii below ~35 μm for quasi-TE modes, for which total losses as low as 0.02 dB/90° have been calculated for a wide range of radii, which can be tuned by properly selecting the thickness of the buffer layer. A more modest decrease of the total losses has been obtained for the quasi-TM modes for radii between 3 and 10 μm. By choosing the right structural parameters, the introduction of the thin metallic layer permits to decrease the optimum bend radius from ~70 μm (i.e., in the entirely dielectric structure) to less than 10 μm while maintaining the total bend loss performance at ~0.02 dB/90°.

In TE polarization, the reduction of the total bend losses can be attributed to the shielding of the mode by the metal layer, which prevents it from leaking into the substrate. The mechanism for the reduction of bend losses is different in TM polarization, for which the higher confinement of the hybrid plasmonic-photonic mode to the metal layer permits decreasing the radius of curvature before coupling to radiation modes occurs.

The approach considered in this paper is quite promising, as it allows the use of polymer waveguides in large-scale photonic integration where sharply bent waveguides with radii of a few micrometers are essential to shrink the footprint of photonic circuitry.

Acknowledgments

The authors acknowledge support from the FP7 Marie Curie Career Integration Grant PCIG09-GA-2011-29389 and the University of Twente Aspasia fund. M. Hammer, H. J. W. M. Hoekstra, R. Stoffer, D. J. Dikken and J. Herek are thanked for useful discussions and advice.

#198328 - $15.00 USD Received 26 Sep 2013; revised 15 Nov 2013; accepted 17 Nov 2013; published 25 Nov 2013